

~~1080~~  
~~27~~  
~~Copy~~

*L. Lang, J. M. A. L.*

TECHNICAL MEMORANDUMS  
NATIONAL ADVISORY COMMITTEE FOR AERONAUTICS

---

No. 762

---

EFFECT OF AERODYNAMIC DESIGN ON GLIDER PERFORMANCE

By A. Lippisch

Luftfahrtforschung  
Vol. 11, No. 5, October 25, 1934

---

Washington  
January 1935

1.7.1.3



NATIONAL ADVISORY COMMITTEE FOR AERONAUTICS

TECHNICAL MEMORANDUM NO. 762

EFFECT OF AERODYNAMIC DESIGN ON GLIDER PERFORMANCE\*

By A. Lippisch

SUMMARY

The performance of a glider is determined by means of the velocity polar, which represents the connection between horizontal and sinking speed. This relationship is analyzed. The mean sinking speed for a given speed range can be determined on the basis of the velocity polar. These data form the basis for the most propitious design of a performance-type glider with a view to long-distance flight. It is seen that above all, those gliders are preferable which, with high-wing loading, are designed for optimum gliding angle.

The development of the performance gliders of the D.F.S. (German Research Institute for Gliding) is discussed with special reference to the design of the "Fafnir II", and the performances of the "Obs" are compared with those of the "Fafnir II".

1. NOTATION

G,	flight weight	kg
F,	wing area	m <sup>2</sup>
b,	span	m
A,	$b^2/F$ = aspect ratio	
$\rho$ ,	air density	kg m <sup>-3</sup> s <sup>2</sup>
v,	path velocity	m/s
v,	path velocity	
v <sub>x</sub> ,	horizontal speed	m/s

---

\*"Einfluss der aerodynamischen Gestaltung auf die Leistung von Segelflugzeugen." Luftfahrtforschung, October 25, 1934, pp. 122-127.

$v_z$ , sinking speed, m/s

$v_m$ , mean flight speed, m/s

$\Delta v$ , speed range

$\left. \begin{array}{l} c_l \\ c_d \end{array} \right\} \begin{array}{l} c_a \\ c_w \\ c_r \end{array} \right\}$  airfoil characteristics

$c_{wi} = \frac{\kappa}{\pi \Lambda} c_a^2$ , coefficient of induced drag

$c_{wp}$ , coefficient of profile drag

$c_{ws}$ , coefficient of parasite drag

$\kappa$ , ratio of induced drag of a given wing to that of an elliptical wing

## 2. SIGNIFICANCE OF VELOCITY POLAR

The performance of a glider is definitely contingent upon the relationship between horizontal speed  $v_x$  and sinking speed  $v_z$ . These velocity components can, as known, be calculated from the polar diagram, as follows:

$$v_x = \frac{c_a}{c_r^{1.5}} \sqrt{\frac{G}{F \frac{\rho}{2}}}$$

$$v_z = \frac{c_w}{c_r^{1.5}} \sqrt{\frac{G}{F \frac{\rho}{2}}}$$

These relations are derived from the equation for steady gliding flight.

In the normal flight range with low lift/drag ratios the resultant differs but very little from the lift, so that we may simply put  $c_r \cong c_a$ . Then the above equations

reduce to:

$$v_x = \frac{1}{c_a^{0.5}} \sqrt{\frac{G}{F \frac{\rho}{2}}}$$

$$v_z = \frac{c_w}{c_a^{1.5}} \sqrt{\frac{G}{F \frac{\rho}{2}}}$$

Now the velocity diagram is readily computed for a given glider from these equations when plotting the sinking speed versus the horizontal speed. Figure 1 illustrates such a velocity diagram (or what may also be called velocity polar). The analysis was based on a conventional glider type. We note the point of minimum  $v_x$  and  $v_z$ . The flight attitude with best gliding angle is shown as the tangent to the velocity polar. With this graph we can determine the best gliding angle relative to the ground with head or tail wind, upcurrent or downcurrent, by shifting the zero point to the point of the prevailing wind velocities. Thus it is seen, for example, that without upcurrent in a tail wind the pilot must pull on the control stick in order to fly as far as possible, while with head wind his flight speed must exceed that for best gliding angle. These interpretations may be extended to any combination. They afford valuable information to the distance flyer, particularly when the special velocity diagram of the glider used is available.

The ensuing analysis of the characteristics of various types of gliders is made on the basis of velocity polars.

Everyone's interest at present is centered on long-distance flying and specifically, distance flight within limited time, since the thermal upcurrents which make such flight possible, are confined to daytime. An ideal distance glider would therefore be one whose sinking speed even at higher flight speed would still be lower than the normal upcurrents, or in other words, whose curve of the velocity polar shows a flat sinking speed minimum and a slow sinking speed rise toward higher speeds. Obviously this requirement is primarily coincident with optimum lift/drag ratios, as becomes particularly clear when comparing a glider with low wing loading and low  $\Lambda$ , to one having a high wing loading and a high  $\Lambda$  (fig. 2). The calculation was so made that both gliders have the same minimum  $v_z$ . In spite of the fact that the velocity

polar of the glider with low wing loading had been calculated with extremely favorable figures, the comparison is unfavorable for this type, because of its much faster increasing sinking speed than for the other type with high wing loading and aspect ratio.

As second comparison, we analyze the velocity polars of the same airplane but with different wing loadings (fig. 3). In this case the airfoil characteristics remain the same, but the scale of the velocity polars becomes different, i.e., the polars reveal mutual affinity because the points of equal lift coefficients lie on radii through the origin. A study of the sinking speeds at higher flight speed discloses them as becoming less as the wing loading increases, since in this case the favorable range of the velocity polars gains prevalence. Consequently, in order to assure the best sinking speed for a certain speed, the glider must be so loaded that it then flies with best gliding angle. This is readily seen from figure 3, because the tangent to the velocity polar characterizes the limit of the sinking speed.

In the third scale of comparison the gliders have equal wing loading and aspect ratio but are unlike in parasite drag (fig. 4). Apart from the improved minimum sinking speed the salient feature is the substantially less steep course of the velocity polars as a result of the decreased frontal drag. So, having previously conceded this configuration of the velocity diagram to be propitious, we now can confirm that decreasing the parasite drag and raising the wing loading, is conducive to better distance performance.

Lastly, since the decrease in induced drag is generally interpreted as a reduction in total drag, one might assume that this line of attack would perhaps yield further advantages. But, bearing in mind that the effect of the induced drag depends on the lift coefficient, no substantial improvement from the aspect ratio could be expected, save in the range of high lift coefficients, i.e., but in the ambit of low speeds. Figure 5 illustrates such a comparison. Thus it is seen that the principal effect of the improvement through aspect ratio is on the minimum of the sinking speed. In order to make this difference visible at all, we chose a great difference between the various aspect ratios.

After thus outlining the essential influences on the shape of the velocity polars, we analyze these factors separately. To this end, we develop the velocity diagram with reference to the airfoil characteristics, the wing loading, and the span loading. The polar diagram can be expressed with

$$c_w = \frac{\kappa c_a^2}{\pi \Lambda} + c_{wp} + c_{ws}.$$

The first term denotes the induced drag effect, the second is the profile drag, which is also a function of the lift coefficients, whereas the third term represents the residual drag which is substantially constant over the lift range. The addition of the equations for  $v_x$  and  $v_z$  then gives

$$v_z = \frac{\kappa G}{\pi F \frac{\rho}{2}} \frac{1}{v_x} + (c_{wp} + c_{ws}) \frac{\frac{v_x^3}{G}}{\frac{F \frac{\rho}{2}}{1}}$$

Bearing in mind that

$$\frac{G}{\Lambda F} = \frac{G}{b^2},$$

we have:

$$v_z = \frac{\kappa}{\pi} \frac{G}{\frac{\rho}{2}} \frac{1}{b^2} \frac{1}{v_x} + \frac{(c_{wp} + c_{ws})}{\frac{G}{F \frac{\rho}{2}}} v_x^3$$

Here it should be remembered that profile drag coefficient  $c_{wp}$  is dependent on the lift coefficient and consequently also on the horizontal speed  $v_x$ . As a result, the sinking speed for a certain speed may be divided into three parts, namely, that of the induced drag, the profile drag, and the parasite drag. This becomes particularly clear when following the course of the three parts in a velocity diagram (fig. 6). The effect of the induced drag is, as expected, negligible at higher flight speeds. Contrariwise, the profile drag is most pronounced at higher speeds, and the parasite drag also predominates in this

range by a multiple of the induced drag. Consequently, to design a glider suitable for distance flight means above all, to cut down on profile drag and parasite drag.

### 3. THE OPTIMUM DESIGN OF PERFORMANCE GLIDERS

The deciding condition for the long-distance glider may now be formulated as follows:

A glider should be so designed that the mean sinking speed in a certain speed range becomes minimum.

The structural requirement can be deduced from the relation between  $v_x$  and  $v_z$ . With  $v_m$  = mean flight speed and  $\Delta v$  = speed range, the mean sinking speed is:

$$v_{z_m} = \frac{1}{\Delta v} \int_{v_m - \frac{\Delta v}{2}}^{v_m + \frac{\Delta v}{2}} v_z \, dv$$

which, integrated, gives:

$$\begin{aligned} v_{z_m} = \frac{1}{\Delta v} & \left[ -\frac{\kappa}{\pi} \frac{G}{\rho} \frac{1}{b^2} \ln \left( \frac{2v_m + \Delta v}{2v_m - \Delta v} \right) \right. \\ & + \frac{c_{ws}}{G/F} \frac{\rho}{2} \left( v_m^3 \Delta v + \frac{v_m}{4} \Delta v^3 \right) \\ & \left. + \frac{\rho/2}{G/F} \int_{v_m - \frac{\Delta v}{2}}^{v_m + \frac{\Delta v}{2}} c_{wp} v_x^3 \, dv \right] \end{aligned}$$

From this equation, the best  $G/b^2$  and  $G/F$  can then be determined for a certain speed range based on a mean speed. For approximations the profile drag may be introduced as invariable within the pertinent range, so that,

$$c_{ws} + c_{wp} = c_{wm}.$$

Then the mean sinking speed is:

$$v_{zm} = \frac{1}{\Delta v} \left[ A \ln \left( \frac{2v_m + \Delta v}{2v_m - \Delta v} \right) + B \left( v_m^3 \Delta v + \frac{v_m}{4} \Delta v^3 \right) \right]$$

wherein

$$A = \frac{\kappa \frac{G}{b^2}}{\pi \frac{\rho}{2}} = \frac{\kappa \frac{G}{F}}{\pi \Lambda \frac{\rho}{2}}$$

and

$$B = \frac{c_{wm} \frac{\rho}{2}}{\frac{G}{b^2} \Lambda} = \frac{c_{wm} \frac{\rho}{2}}{\frac{G}{F}}$$

The best wing loading is:

$$(G/F)_{\text{best}} = \frac{\rho}{2} \sqrt{\frac{c_{wm} \pi \left( v_m^3 \Delta v + \frac{v_m}{4} \Delta v^3 \right)}{\kappa \ln \left( \frac{2v_m + \Delta v}{2v_m - \Delta v} \right)}}$$

According to last year's experiences, the speed range in distance flights should chiefly lie between 50 and 70 km/h (31.7 and 43.5 mi./hr.) (fig. 7). This diagram gives a survey of the relationship between wing loading, aspect ratio, and drag coefficient. It shows that an increasing aspect ratio and drag coefficient calls for a higher wing loading. Since the average drag coefficients of gliders are about of the order of size of 0.02 to 0.03, it is readily seen that at present we operate with a too low wing loading to the detriment of distance performance. From the relationship existing between  $G/F$ ,  $\Lambda$ , and  $c_w$ , the mean  $v_z$  may be determined, thus making it possible to

plot the lines of equal mean sinking speed, and to insure between  $G/F$ ,  $v_{zm}$ , and  $\Lambda$ , a simple linear relationship characterized by

$$\frac{G}{F} = v_{zm} \Lambda \frac{\rho/2}{\pi \kappa} \frac{\Delta v}{2 \ln \left( \frac{2v_m + \Delta v}{2v_m - \Delta v} \right)}$$

The lines of equal sinking speed are shown as straight lines, and the whole interdependence of the essential gliding parameters is now visible. The graph (fig. 7) was plotted for the speed range between 50 and 70 km/h. Obviously, a different speed range changes the diagram, the wing loading increasing with higher mean speed. As this development is desirable in order to raise the distance performance, the demand for higher wing loading ranks, of course, first. An improved aerodynamic glider design stipulates a certain compensation for, according to the diagram, a saving in drag demands a reduction in wing loading. In more detailed investigations of these relations, the dependence of profile drag on the lift coefficient must be taken into consideration, which means that the particular integral must be individually evaluated. The evaluation based upon a definite polar diagram, starts with the separation of the coefficients decisive for  $v_x$  and  $v_z$ . In this fashion an absolute velocity polar may be established whereby  $c_w/c_a^{1.5}$  is shown against  $1/c_a^{0.5}$ . Then

$$\frac{c_w}{c_a^{1.5}} = \frac{\kappa}{\pi \Lambda} c_a^{0.5} + \frac{c_{wp}}{c_a^{1.5}} + \frac{c_{ws}}{c_a^{1.5}}.$$

With  $\frac{1}{c_a^{0.5}} = x$  and  $\frac{c_w}{c_a^{1.5}} = y$ , we obtain, similarly to the velocity polar, an equation:

$$y = \frac{\kappa}{\pi \Lambda} \frac{1}{x} + c_{wp} x^3 + c_{ws} x^3.$$

The absolute speed range is determined by the boundary

$$x_1 = \frac{1}{c_{a1}^{0.5}}$$

and

$$x_2 = \frac{1}{c_{a2}^{0.5}}$$

Subsequent integration of the mean sinking speed coefficient then shows the same form as the determination of  $v_{zm}$ .

4. The "Fafnir I", "Obs", and "Fafnir II", of the D.F.S.

It is only by grasping these relationships that we can understand the trend of development followed by D.F.S. for several years in its attempt to promote the design of long-distance gliders. The first of these was the "Fafnir I": departing from conventional practice - parasol wing separate from fuselage - in favor of the high wing with fillets. This typical wing shape (tapered tip with pronounced aerodynamic twist) was decided upon from practical and structural reasons. Save for the cockpit cowl introduced for the first time, the high wing would have been impossible because the cockpit cut-out would have resulted in serious aerodynamic disadvantages. It was generally believed at that time that the best aerodynamic design was obtainable only with wing separate from the fuselage. But from my own aerodynamic investigations on gliders, I found that with a semihigh-wing design it was possible to reduce the body drag.

Figure 8 shows a glider which I designed in 1921, and even though the results were negative due to structural defects, the aerodynamic aspect was noteworthy for that time. The correct fairing of the fuselage into the wing is characterized by the low additive body drag. The first attempt on the "Fafnir I" was unsuccessful. Muttray's investigations explained this problem very thoroughly and proved that this line of attack would unquestionably be successful. The logical result was the new type "Fafnir II". The intermediate type, the "Präsident", is patterned after the studies of 1921. On the "Fafnir II" we abandoned the semihigh wing in favor of the mid wing, which was preferable according to Muttray's investigations. The shape of the wing itself was subject to other and very elaborate experiments.

The aim was to establish the extent of the aerodynamic twist of the wing necessary to obtain adequate maneuverability in turns. Whereas the choice of airfoil for the "Fafnir I" was made from general points of view, the new aerodynamic study according to airfoil theory, produced some very remarkable results and showed that for

purposes of maneuverability in turns, the "Fafnir" wing needed considerable twist. All in all, it was possible to theoretically define each section so that the complete outer form of the new glider could be constructed in accord with airfoil theory and Birnbaum's airfoil analysis. The intended aerodynamic study of the model glider itself had to be postponed, since we had barely five months available in which to build the glider. Figures 9-15 show the "Fafnir II" in various stages of construction.

The flight performance was determined from test flights with several types of gliders fitted with recording altimeter and dynamic pressure recorder, while the airplane used for towing, carried a meteorograph for recording pressure, temperature, and humidity. The flights were usually made in the early morning hours to avoid as much as possible any falsification of the measurements due to vertical air movements. The glider pilot flew in stages at different dynamic pressures so that the sinking speed at different flight speeds, i.e., the velocity polar itself, could be determined. The slope of the barograph curve was established from the barogram and the height loss in time rate, that is, the sinking speed computed for the air density prevailing at that height.

With a standard density of  $\rho_0 = 0.125$  as basis, the dynamic pressure and the recorded sinking speed were then extrapolated and plotted in the velocity diagram, from which the pertinent points of the polar diagram were obtained. Figures 16-21 show the results of flight measurements for the two-place glider "D - Obs", and glider "D - Sao Paulo" ("Fafnir II"). The polars are compared in figure 21. The superior aerodynamic design of the "Fafnir II" is readily noted, particularly in the upper range of the polar.

Obviously the method of measurement discussed here needs to be considerably improved upon in the future. This applies in particular to the instruments used at present, which for the special purpose of such measurements, are far too inaccurate.

However, this method is practical in principle. It should make it possible to determine the airfoil characteristics of any glider design and thereby afford valuable information not only for the limited range of gliding but for aviation in general.

Translation by J. Vanier,  
National Advisory Committee for Aeronautics.

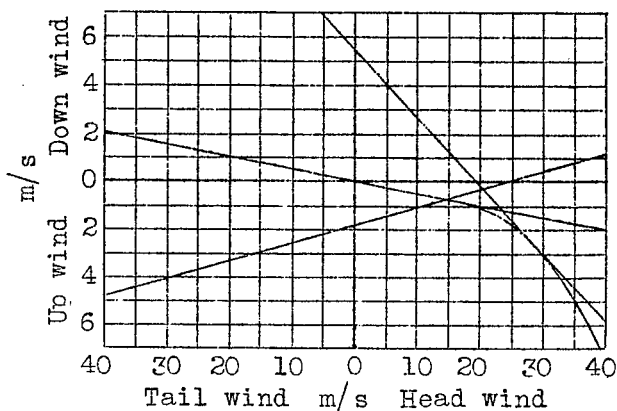


Figure 1.-Velocity polar.

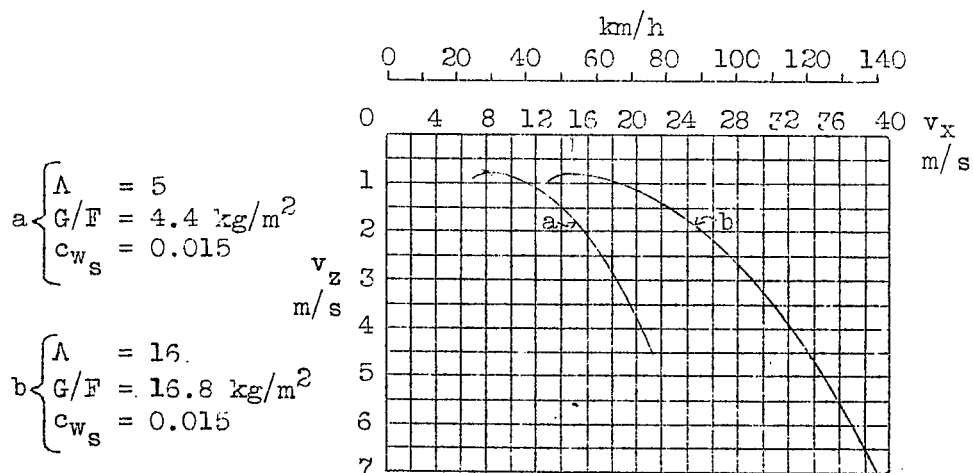


Figure 2.-Different aspect ratio with equal sinking-speed minimum.

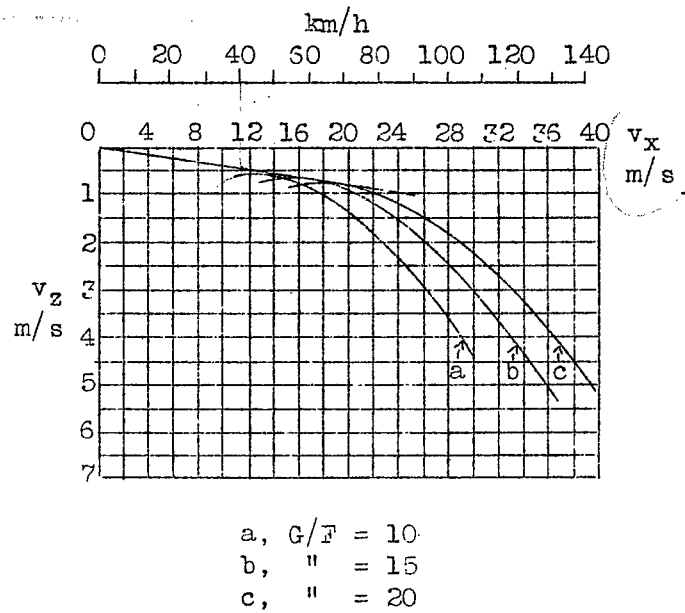


Figure 3.-Effect of wing loading.

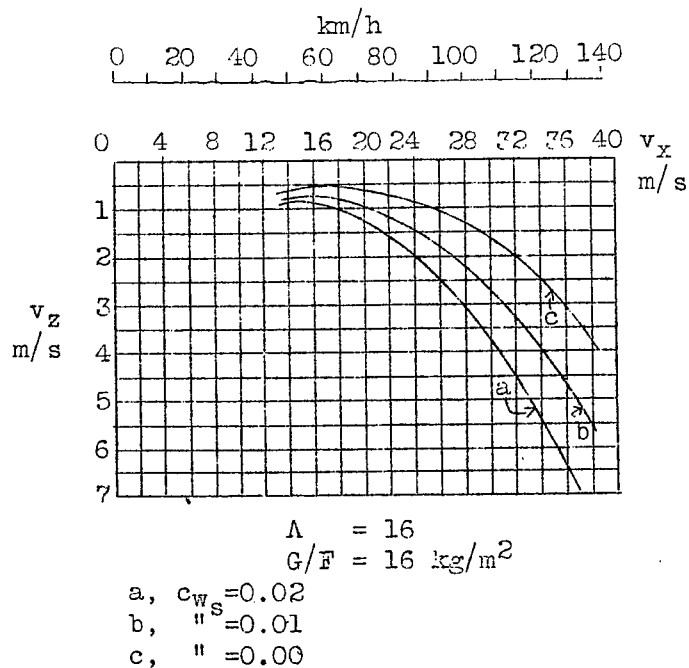
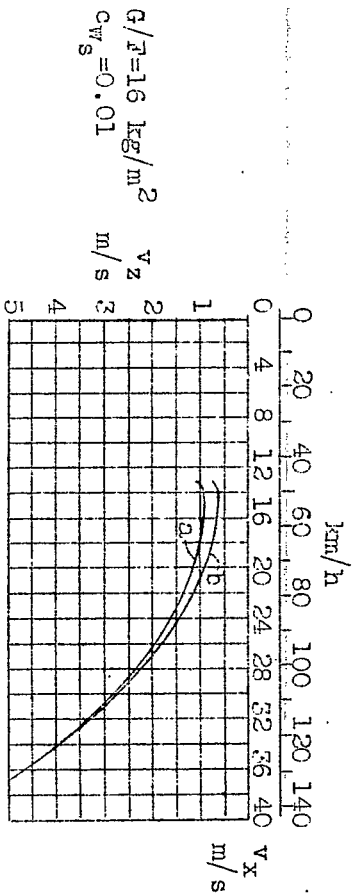


Figure 4.-Effect of parasite drag.



a,  $\Lambda = 16$   
 b,  $\Lambda = 20$   
 Figure 5.-Effect of aspect ratio.

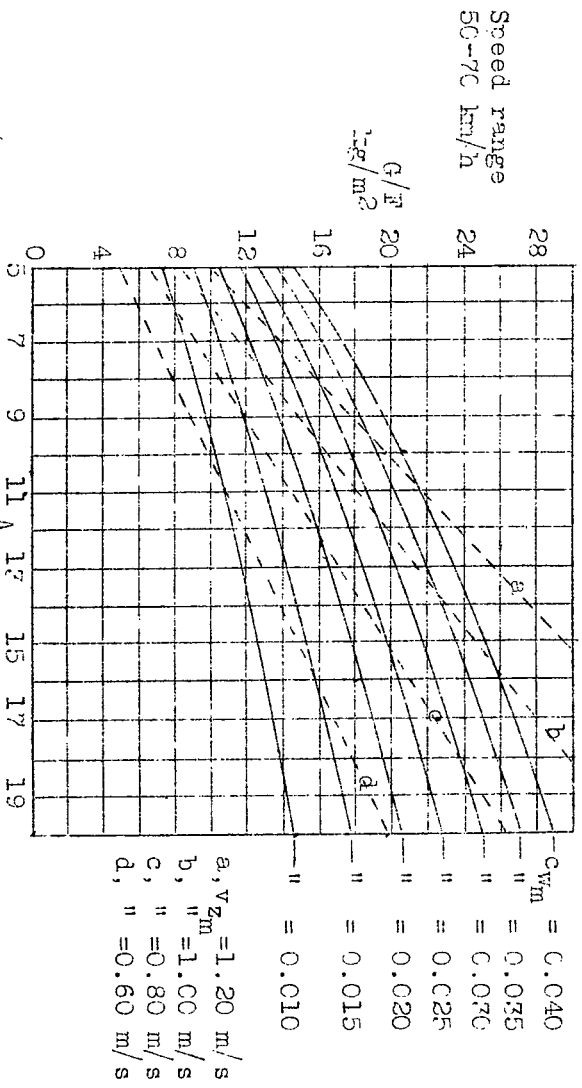


Figure 7.-Optimum values for the long-distance glider.

$$\left[ \frac{G}{\bar{F}} \right]_{\text{best}} = \frac{\rho}{2} \sqrt{\left( \frac{c_{wm}}{K} \right) \pi \Lambda \left( \frac{V_m^3 \Delta v + \frac{V_m}{4} \Delta v^3}{\ln \left( \frac{2V_m + \Delta v}{2V_m - \Delta v} \right)} \right)}$$

$$\left[ \frac{G}{\bar{F}} \right]_{\text{best}} = V_{zm} \Lambda \pi K \frac{\rho/2}{2 \ln \left( \frac{2V_m + \Delta v}{2V_m - \Delta v} \right)}$$

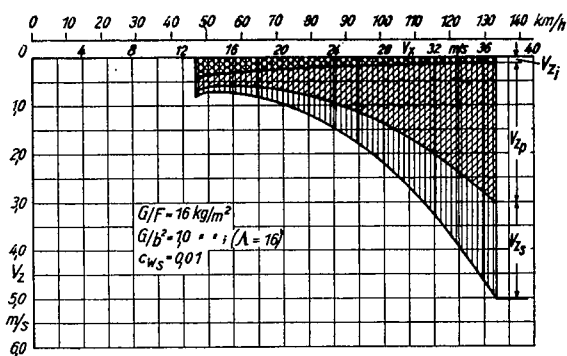


Figure 6.- Division of velocity polar.

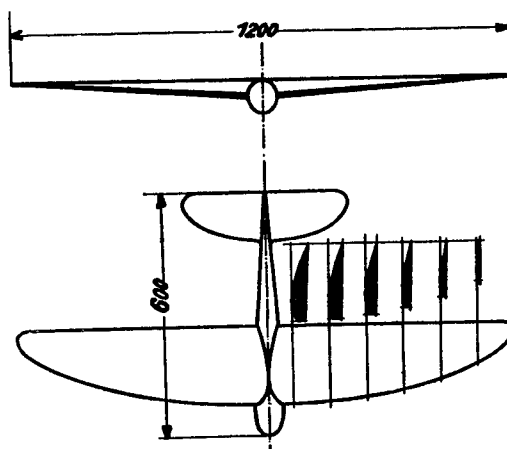


Figure 8.- Model measurement of 1921.

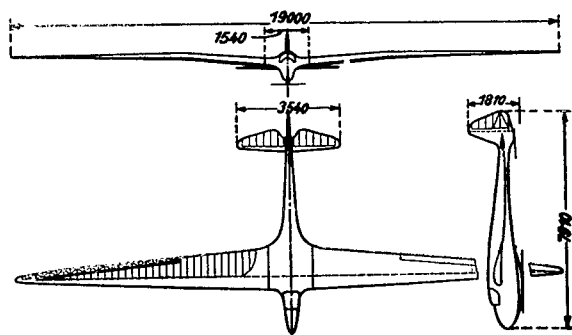


Figure 9.- Three-view drawing of D São Paulo (Fafnir II).

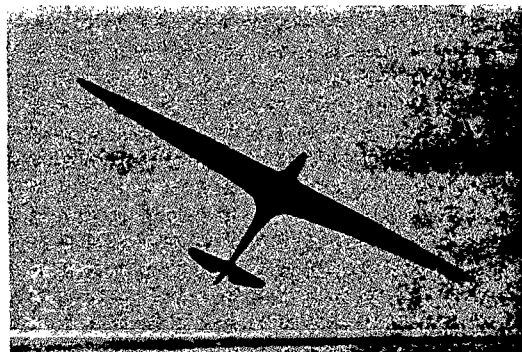


Figure 16.- D-São Paulo in flight.



Figure 10.- Maximum cross-section and wing attachment fittings of D São Paulo (front view)



Figure 11.- Wing under construction.

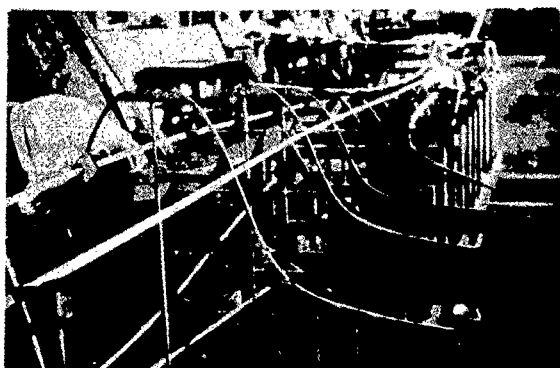


Figure 12.- Fuselage under construction.



Figure 13.- Wing-fuselage fillet under construction (rear view)



Figure 14.- Wing-fuselage fillet finished (rear view)

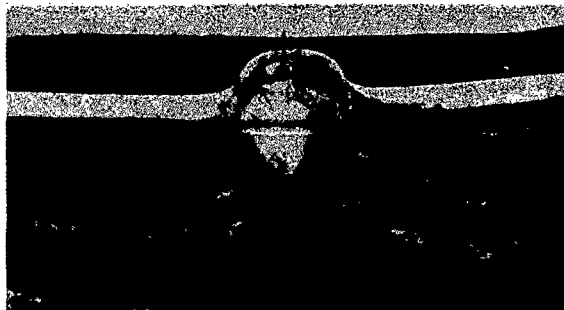


Figure 15.- Wing-fuselage fillet finished (front view)

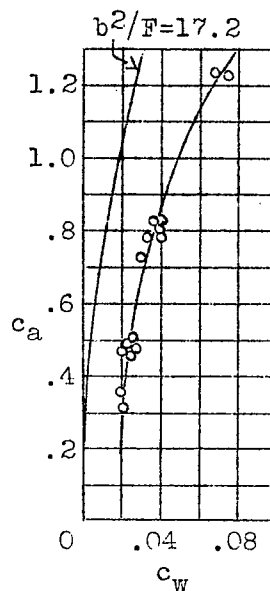


Figure 17.-Polars of "D-Obs" recorded in flight.

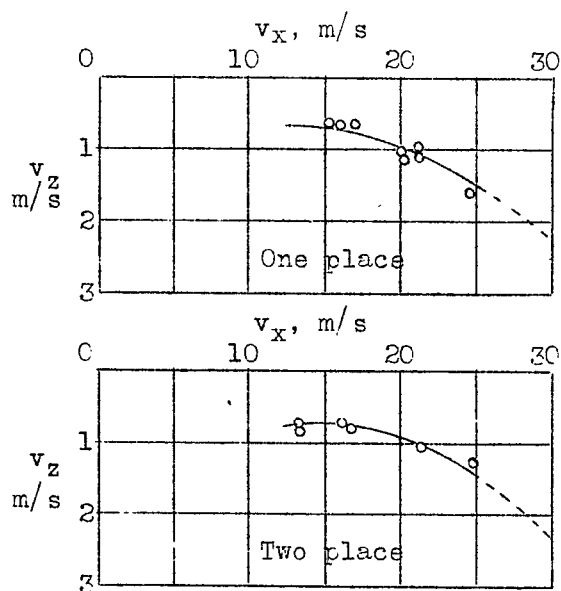


Figure 18.-Velocity polar of "D-Obs" recorded in flight.

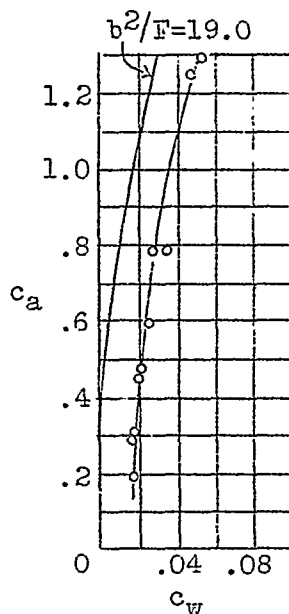


Figure 19.--Flight record of "D-Sao Paulo" polar.

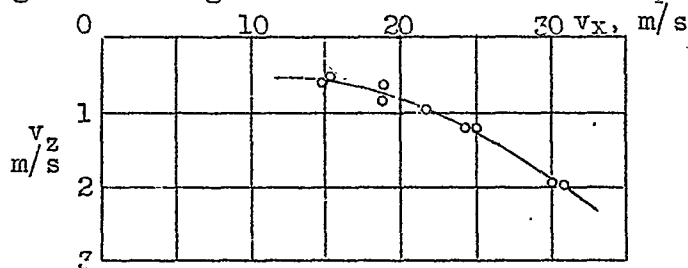


Figure 20.--Flight record of "D-Sao Paulo" velocity polar.

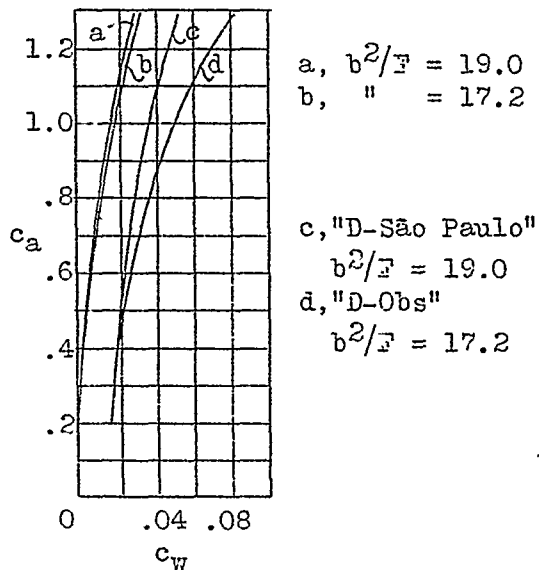


Figure 21.--Comparison of polars of "D-Obs" and "D-São Paulo".

NASA Technical Library



3 1176 01441 1491